Progress In Electromagnetics Research B, Vol. 28, 219–234, 2011

CONTRAST ENHANCED BEAMFORMING FOR BREAST CANCER DETECTION

D. Byrne, M. O'Halloran, M. Glavin, and E. Jones

College of Engineering and Informatics
National University of Ireland Galway
University Road, Galway, Ireland

Abstract—The early identification of malignant tissue is one of the most significant factors in the successful treatment of breast cancer. Microwave imaging is an emerging breast screening modality based on the dielectric contrast between normal and cancerous tissues at microwave frequencies. When the breast is illuminated with an Ultrawideband (UWB) microwave pulse, the dielectric contrast between normal and cancerous tissues generates electromagnetic reflections. These reflected signals, containing tumor backscatter, are spatially focused using a beamformer which can compensate for attenuation and phase effects as the signal propagates through the breast. However, recent studies have shown the breast to be a dielectrically heterogeneous entity. High levels of heterogeneity reduce the dielectric contrast between normal and cancerous tissue, limiting the effectiveness of beamforming algorithms. One possible method to assist in the diagnoses of cancer in a heterogeneously dense breast is the use of contrast agents. Contrast agents modify the dielectric properties of a malignant tumor site in order to increase the dielectric contrast with fibroglandular tissue. In this paper, a number of beamforming algorithms are applied to MRI-derived models with endogenous and contrast enhanced malignant tissue properties. Two contrast agents are applied to heterogeneously dense breast phantoms and simulations are carried out prior and post contrast agent delivery. A range of tumor diameters are simulated and a number of beamforming algorithms are applied to the simulated data. The resulting differential scans are then compared across a range of appropriate metrics.

Received 8 December 2010, Accepted 9 February 2011, Scheduled 12 February 2011
Corresponding author: Dallan Byrne (dallanbyrne@gmail.com).

1. INTRODUCTION

The significant number of new cases of breast cancer reported globally (1.5 million in the US alone [1]), coupled with the limitations of the current *de facto* breast cancer screening method, X-Ray Mammography [2, 3], have prompted the investigation of alternative breast imaging modalities.

Microwave imaging is one such promising breast imaging modality, using backscattered radar signals to identify cancerous regions within the breast [4, 5]. The dielectric contrast between tissue types, notably malignant and normal breast tissues, generate electromagnetic reflections within the breast. These reflections can be recorded and a time-domain image-formation algorithm (beamformer) can be used to determine the location of any dielectric scatterer present.

Recently established data on the dielectric properties of the breast [6] has shown that:

- The level of dielectric heterogeneity within the breast had previously been significantly underestimated.
- The dielectric contrast between fibroglandular tissue and cancerous tissue was less than 10%.

These findings highlight the challenges associated with using microwave imaging to locate cancerous regions within a heterogeneously dense breast, which contains significant fibroglandular tissue content [7, 8]. Contrast agents have been shown to modify the relative permittivity and conductivity of tissue-mimicking materials [9]. Using these agents, the contrast between fibroglandular and malignant tissue can be controlled in order to accurately locate tumors within the breast.

In this paper, the effectiveness of tumor localization in contrast enhanced differential images is examined using the following beamforming algorithms: Delay-And-Sum (DAS) [4, 10], Delay-Multiply-And-Sum (DMAS) [11], Improved Delay-And-Sum (IDAS) [12] and Transmitter-Grouping Robust Capon Beamforming(TGRCB) [13]. Each algorithm is evaluated using an anatomically realistic breast model with a tumor of varying diameter, located in a region of dense fibroconnective tissue. Differential images are then obtained by calculating the energy differences between images which are prior and post contrast agent application. A number of metrics are used on the differential scans to determine the quality and effective localization ability of each beamforming algorithm.

The remainder of the paper is organized as follows: Section 2 describes the four beamforming algorithms used to obtain differential energy scans. The use of contrast agents in microwave medical

imaging is considered in Section 3. The numerical breast model model and performance metrics are described in Section 4, and results are presented in Section 5. Finally, conclusions and suggestions for future work are discussed in Section 6.

2. IMAGING ALGORITHMS

Beamforming algorithms can be classified as: Data-Independent or Data-Adaptive methods. Data-Independent beamformers use an assumed propagation model to compensate for path dependent attenuation and dispersion [4, 7, 8, 10–12]. Conversely, Data-Adaptive algorithms process the received signals in order to achieve unit gain from a desired direction, while suppressing signals of the same frequency from all other directions [13–15]. The Delay-And-Sum (DAS) beamformer is based on the Confocal Microwave Imaging approach [4]. The DAS algorithm time-shifts and sums the backscattered signals from the breast to create a synthetic focus. If a tumor exists at a specific focal point, then the returns from the tumor site will add coherently. Returns from clutter due to variations in tissue types will add incoherently, and therefore will be suppressed. The energy at this synthetic focus is measured and stored, and an image of energy scattered by breast tissue is created by varying the position of the synthetic focus within the breast.

Klemm et al. [12] attempted to improve the traditional DAS beamformer by introducing an additional weighting factor, called the Quality Factor (QF), which is a measure of the coherence of UWB backscattering at a particular focal point within the breast. At the focal point ($\mathbf{r}$), energy is collected across a window for each multistatic signal and stored. The energy from the focal point is then cumulatively summed and plotted against the number of channels used in the process. A second order polynomial is fitted to the normalized energy collection curve ($y = ax^2 + bx + c$) with a assumed to be the Quality Factor. a is then multiplied by the voxel energy calculated by the DAS algorithm.

Another variant of the DAS algorithm is the Delay-Multiply-and-Sum (DMAS) beamformer developed by Lim et al. [11]. This algorithm involves signals being time-shifted (as in DAS), multiplied in pairs and their products summed in order to calculate the energy at a focal point.

The Data-Adaptive Transmitter-Grouping Robust Capon Beamformer (TGRCB) [13] attempts to determine the power of a desired waveform by using received signal data to vary weights (via a steering vector) applied to the antenna array [14, 15]. The TGRCB method uses a unique signal grouping method, in order to effectively and efficiently

apply the RCB algorithm. For each transmitter, all the corresponding received signals are grouped together and the RCB method is applied to this data set.

3. CONTRAST AGENTS

Confocal Microwave Imaging (CMI) is based on a number of assumptions about the dielectric properties of the breast: that the breast is primarily dielectrically homogeneous and that there exists a significant dielectric contrast exists between cancerous and normal breast tissue. Therefore, as suggested by Lazebnik et al. [6], dense breast tissue, where there is a significant concentration of fibroglandular tissue, poses significant challenges to UWB radar imaging methods. One possible solution is the use of contrast agents.

The Enhanced Permeability and Retention [16] of malignant tissue ensures that the clearance of macromolecules or lipids from a tumor site is significantly impaired compared to normal or inflamed tissue. Certain macromolecular substances can selectively target tumors and remain at high concentration at the tumor site after clearing from nearby organs and tissues. A number of chemical agents have been observed to significantly modify the dielectric properties of tissue mimicking materials. Microbubble solutions have been shown to lower the relative permittivity and conductivity of a specimen by over 30%, at certain controlled volumes [17]. Another promising nongaseous contrast agent is Single-Walled Carbon Nanotubes (SWCNT) [18]. A recent study has shown that SWCNT can increase both the relative permittivity and effective conductivity by up to 22% and 61% respectively [19]. SWCNTs have been successfully chemically conjugated with drug delivery antibodies in order to target the contrast agent towards a tumor site without altering its core functionality [20].

The use of contrast agents in clinical imaging is carried out as follows: An initial UWB image of the breast is created. A contrast agent is delivered and accumulates at the tumor site. The breast is then re-imaged and the energy difference between the prior and post agent delivery scans is calculated. The tumor site may be visible in the resultant differential image due to the dielectric difference between the cancerous tissues, before and after contrast agent application. This paradigm is also used in this study.

4. SIMULATIONS AND EVALUATION METRICS

4.1. Numerical Simulations

Simulation data is obtained by generating 3-D Finite Difference Time Domain (FDTD) models of the breast. Each FDTD model is based on an MRI-derived breast model, taken from the UWCEM breast phantom repository, University of Wisconsin-Madison [21]. The intensity of each voxel in the MRI is estimated and mapped to appropriate dielectric properties in the resultant FDTD model [21]. In order to adequately evaluate the effectiveness of the contrast agents, a heterogeneously dense breast is considered, as shown in Figure 1.

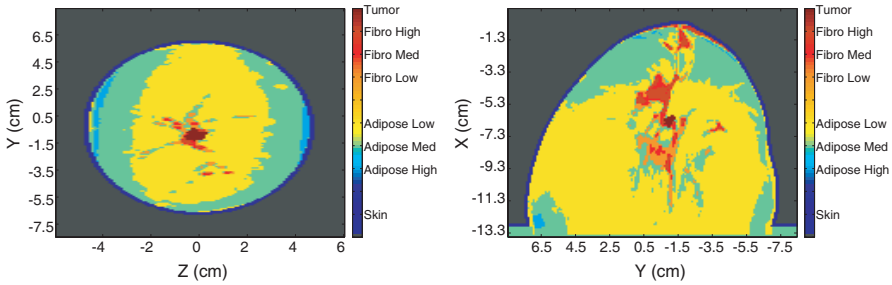

Figure 1. Breast tissue model with a 8 mm tumor at (−6.9, −1, −0.2). (a) Slice taken at $X = -6.9$ cm for Y-Z image and (b) at $Z = -0.2$ cm for X-Y image.

Dimensions within the 3D region of the breast are described according to each axis. The X axis signifies the depth of the breast, with 0 cm indicating the anterior position. Y and Z represent the span and breadth of the breast respectively, with 0 cm centered at the midpoint of each. A microlobulated sphere, representing a malignant tumor, is introduced into the FDTD model. The tumor is positioned at location (−6.9, −1, −0.2) in each simulation, where a particular location within the breast is represented as $((X(\text{cm}), Y(\text{cm}), Z(\text{cm}))$. Tumor models are generated using the Gaussian Random Spheres method [22–24] to simulate realistic shapes and surface textures. The variation of tumor size is simulated by modifying the sphere radius, generating tumors of 2 mm, 4 mm, 8 mm and 12 mm diameters.

The dispersive properties of breast tissue are incorporated into the FDTD model using a single-pole Debye model [25] of the following form:

$$\epsilon_r(\omega) = \epsilon_\infty + \frac{\sigma}{j\omega\epsilon_0} + \frac{(\epsilon_s - \epsilon_\infty)}{1 + j\omega t_0} \tag{1}$$

where ϵ_s is the static permittivity, ϵ_∞ is the permittivity at infinite frequency, ϵ_0 is the permittivity of free space, σ represents the conductivity and t_0 is the relaxation time. The dielectric properties of adipose and fibroglandular tissue are based on the results presented by Zastrow et al. [21]. Skin debye parameters are obtained from published data by Gabriel et al. [26]. Finally, Debye values for cancerous tissue, as well as the Microbubble and SWCNT-infused tumour tissue are taken from Shea et al. [27]. To simulate the modified dielectric properties of the air-filled microbubbles, the relative permittivity and conductivity of an endogenous tumor is reduced by 30% [17]. SWCNTs are represented by increasing the endogenous tumor's relative permittivity and conductivity by 22% and 66%, respectively [19]. All Debye parameters are described in Table 1.

Table 1. Debye parameters for the FDTD model.

Tissue	ϵ_∞	$(\epsilon_s - \epsilon_{\text{inf}})$	σ	t_0
Skin	15.63	8.2	0.82	12.6
Adipose (Low)	2.85	1.10	0.025	13
Fibroglandular (Low)	12.85	24.64	0.251	13
Adipose (Medium)	3.12	1.59	0.050	13
Fibroglandular (Medium)	13.81	35.55	0.738	13
Adipose (High)	3.98	3.54	0.080	13
Fibroglandular (High)	14.28	40.52	0.638	13
Tumor Endogenous	18.8	37.8	0.803	15
Tumor + Microbubble	13.2	26.5	0.562	15
Tumor + SWCNT	69.3	54.5	1.47	15

The overall FDTD grid size is approximately 3.3 million cubic cells, the grid resolution is ($1\,\text{mm}(dx) \times 1\,\text{mm}(dy) \times 1\,\text{mm}(dz)$) and the time step dt is defined as 1.66 ps ($dx/2c$), where c represents the speed of light. The FDTD grid is terminated on each side by a 12 layer Universal Perfectly Matched Layer (UPML) [28] in order to minimize edge reflections. In total, 12 FDTD simulations were carried out, based on three levels of dielectric contrast and four tumor diameters. A cylindrical antenna array [10], consisting of half-wavelength dipole antennas polarized in the direction of the X axis, is placed around the breast. Fifty three antennas are arranged on five rings, as illustrated in Figure 2. The antenna array elements are placed on the skin, with a uniform spacing of 22 mm between each ring along the X

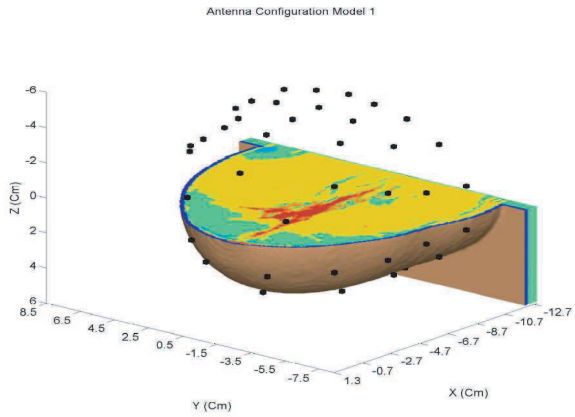

Figure 2. Antenna configuration.

axis. The input pulse is a 120 ps differentiated Gaussian pulse, with a center frequency of 7.5 GHz and a −3 dB bandwidth of 9 GHz. An ideal artifact removal algorithm [7, 13] is applied to the backscattered signals to remove the input signal and any reflection from the skin-breast interface. Prior to any signal processing, all FDTD signals are downsampled to 50 GHz.

4.2. Metrics

Signal to Max ratio (SMXR) and the distance between actual and imaged tumor (D_{rel}) are used in order to evaluate the effect of the contrast agent on the performance of each beamformer. The SMXR is defined as the ratio of the tumor response to the maximum clutter response in the same breast and D_{rel} describes the distance in mm between the actual and imaged tumor peak.

5. RESULTS

Differential profiles, obtained from energy backscatter, represent the energy difference between a beamformed scan with an endogenous tumor and a scan where the dielectric properties of the tumor are modified by the contrast agent. By way of example, Figure 3 illustrates the prior and post contrast enhanced slice along with a resultant differential energy slice. Two contrast agents are applied to the numerical models. This results in two differential images, representing the application of the air-filled microbubbles and the SWCNTs.

Differential imaging beamformer results of a 2 mm and 12 mm contrast enhanced microlobulated tumor are shown in Figures 4 and 5, as a Y-Z and associated X-Y cross-sectional slice. The DAS, IDAS, DMAS and TGRCB algorithms were applied to the numerical data prior to and post application of the air filled microbubbles and the SWCNTs. SMXR results were taken from the 3D scans with endogenous dielectric tumor properties (Table 2) as well as the differential images obtained from the Microbubble (Table 3) and SWCNT (Table 4) enhanced numerical simulations. Furthermore, the D_{rel} results are shown in Table 5.

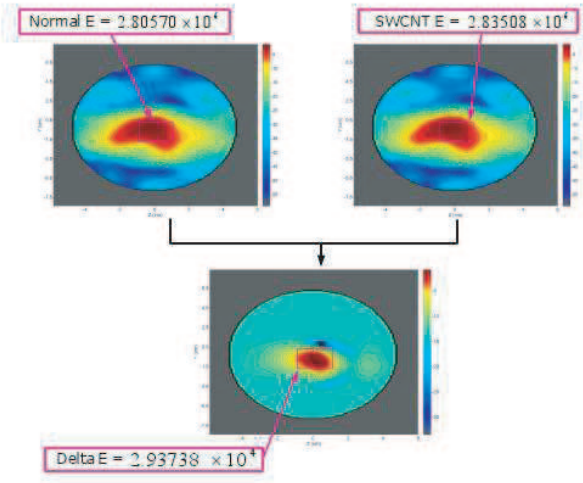

Figure 3. Examples of an endogenous, SWCNT enhanced and resulting differential DMAS image. Energy values are calculated within the pink rectangles, near the actual tumor location at $(6.9, -1, -0.2)$.

Table 2. Signal to Max ratio (SMXR) — results for endogenous tumor images.

Radius(mm)	DAS	IDAS	DMAS	TGRCB
2	−0.44	−0.72	−0.88	0.14
4	−0.33	−0.72	−0.65	1.00
8	0.54	−0.55	1.24	3.96
12	1.83	−0.18	3.73	3.97
Average	**0.40**	**−0.54**	**0.86**	**2.24**

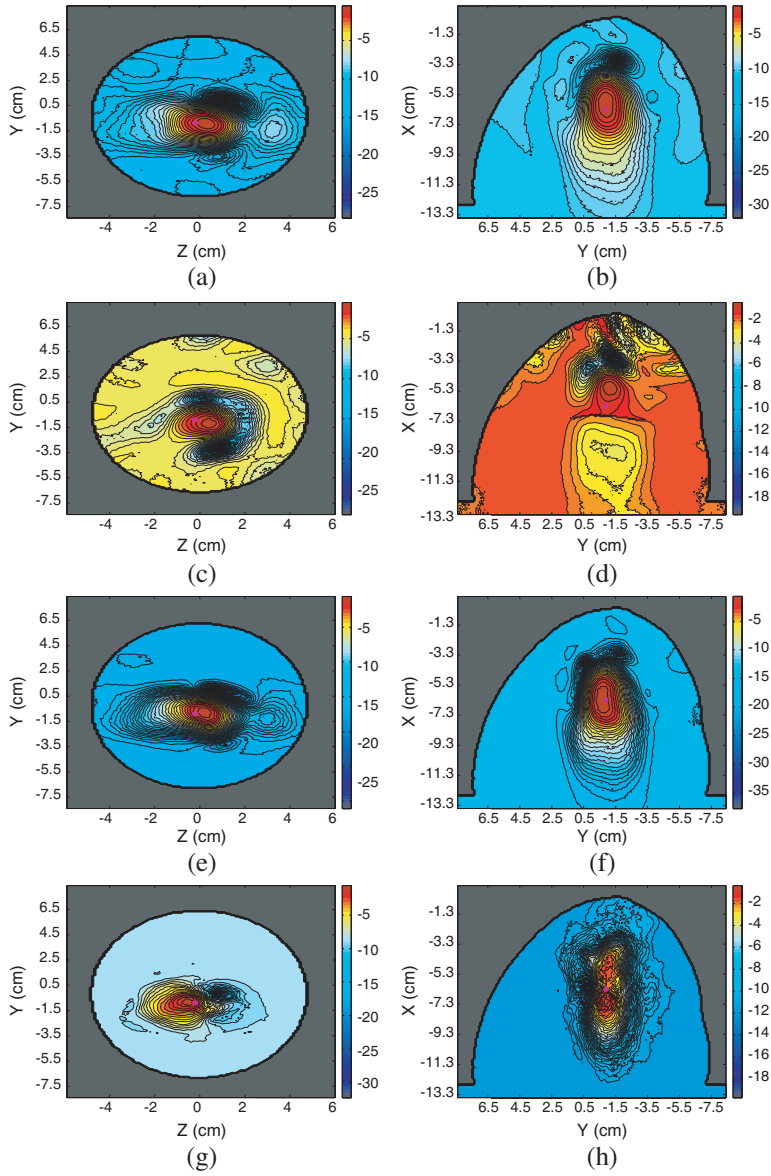

Figure 4. Multistatic beamformed Microbubble differential images for a 2 mm tumor located at $(6.9, -1, -0.2)$. Slices are taken at $X = -6.9$ cm for Y-Z images and $Z = -0.2$ cm for X-Y images. DAS Result (a) and (b); IDAS Result (c) and (d); DMAS Result (e) and (f); and TGRCB Result (g) and (h).

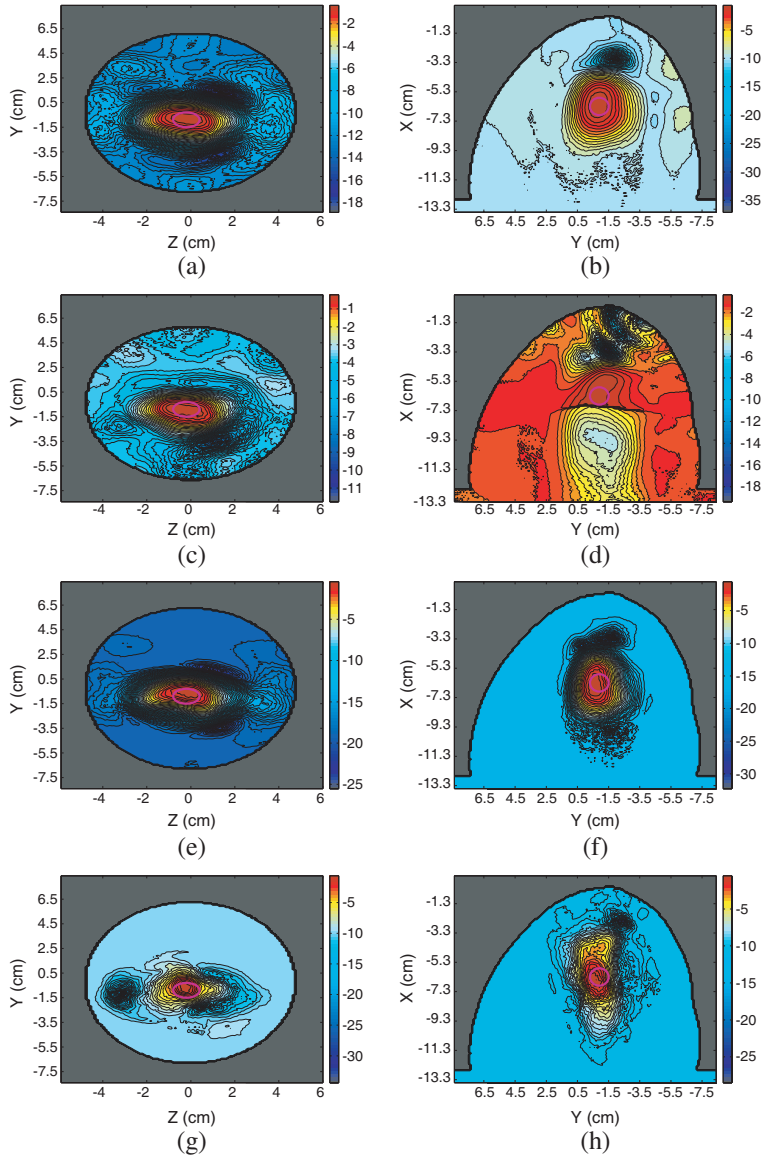

Figure 5. Multistatic beamformed SWCNT differential images for a 12 mm tumor located at $(6.9, -1, -0.2)$. Slices are taken at $X = -6.9$ cm for Y-Z images and $Z = -0.2$ cm for X-Y images. DAS Result (a) and (b); IDAS Result (c) and (d); DMAS Result (e) and (f); and TGRCB Result (g) and (h).

Table 3. Signal to Max ratio (SMXR) — results for microbubble-endogenous differential images.

Radius(mm)	DAS	IDAS	DMAS	TGRCB
2	7.69	3.85	9.67	7.50
4	7.65	4.69	11.04	6.93
8	9.06	4.60	12.53	7.67
12	10.51	3.56	17.76	8.12
Average	**8.73**	**4.18**	**12.75**	**7.55**

Table 4. Signal to Max ratio (SMXR) — results for SWCNT-endogenous differential images.

Radius(mm)	DAS	IDAS	DMAS	TGRCB
2	6.67	5.43	10.47	5.08
4	8.22	5.11	10.98	8.09
8	10.85	2.94	14.23	13.79
12	10.53	3.03	19.88	12.63
Average	**9.07**	**4.13**	**13.89**	**9.90**

Table 5. D_{rel} — Distance between Actual and Imaged Tumor.

Radii	MicroBubbles				SWCNT			
(mm)	DAS	IDAS	DMAS	TGRCB	DAS	IDAS	DMAS	TGRCB
2	5.83	9.38	6.69	5.78	7.81	7.81	7.81	9.85
4	7.28	9.38	6.69	5.78	7.81	9.70	5.92	3.61
8	6.32	6.08	4.12	3.61	5.83	9.70	5.20	3.16
1.2	2.00	7.28	4.69	4.24	8.00	7.81	7.81	3.00
Average	**5.36**	**8.03**	**5.55**	**4.85**	**7.36**	**8.75**	**6.68**	**4.90**

Examining the SMXR results from an imaging scenario containing an endogenous tumor (Table 2), the highest scoring algorithm is the TGRCB, with an average SMXR result of 2.24 dB. IDAS yields the lowest result with an average metric score of −0.54 dB. The DAS and DMAS metrics are comparable, with an average SMXR metric of 0.40 dB and 0.86 dB, respectively.

Examining the SMXR results from an imaging scenario containing an endogenous tumor (Table 2), the highest scoring algorithm is the TGRCB, with an average SMXR result of 2.24 dB. IDAS yields the lowest result with an average metric score of −0.54 dB. The DAS and DMAS metrics are comparable, with an average SMXR metric of 0.40 dB and 0.86 dB, respectively.

As previously reported, all beamformers perform poorly with the presence of fibroglandular tissue. The contrast between the assumed and actual propagation channel affects the performance of each beamformer.

IDAS is the weakest algorithm in this scenario since the beamformer is based on the principle of weighting voxels where coherent addition occurs, and coherent addition occurs, which is much more difficult with increasing levels of dielectric heterogeneity. The TGRCB algorithm significantly reduces clutter in the propagation channel and offers significant improvements over the Data-Independent algorithms.

All SMXR results from differential profiles for both contrast agents (Tables 3 and 4) increase significantly over the endogenous tumour scan results in Table 2. The SMXR results in Table 3 are taken from differential data from microbubble-endogenous scans. DMAS offers the best results with an average SMXR of 12.75 dB, an increase of 11.89 dB from the endogenous scan result. DAS and TGRCB register an average improvement of 8.33 dB and 5.31 dB, respectively. The poorest performer is IDAS, with an average SMXR result of 4.18 dB, giving an improvement of 4.72 dB from the unmodified tumor scan. The results from the SWCNT-Endogenous differential in Table 4 show that DMAS achieves the highest SMXR results, with an average score of 13.89 dB. This is an increase of 13.03 dB over the average endogenous metric result. Again, the IDAS algorithm is the weakest of the four, with an average SMXR of 4.13 dB. The performance of DAS and TGRCB is comparable with an average improvement over the endogenous SMXR metrics of 8.67 dB and 7.66 dB, respectively.

The final Metric, D_{rel} (Table 5), indicates that the TGRCB algorithm achieves the best localization, imaging the malignant tumor closest to the actual tumor location at an average distance of 4.85 mm and 4.9 mm for the microbubble and SWCNT agents, respectively. As with the two previous metrics, the IDAS algorithm performs poorly, recording an average distance of 8.03 mm for a microbubble agent and 8.75 mm in a SWCNT differential image.

The poor performance of the IDAS algorithm can most likely be attributed to the difficultly in compensating for the attenuation effects as the UWB pulse propagates through the heterogeneous breast [8].

The difference between the actual and assumed propagation channel used by the IDAS algorithm means that the cumulative energy curve method is a less reliable measure of coherent addition within a dielectrically heterogeneous breast.

The DMAS algorithm significantly outperforms both the DAS and IDAS algorithm. The DMAS algorithm has previously been shown to perform particularly well when the tumour is the largest scatterer in the breast [7, 8]. When contrast agents are applied, the tumor is an even stronger scatterer due to increased mismatch at the boundary of the malignant inclusion. DMAS performs constructive multiplication at the tumor site, and an improved image of the breast is produced due to the substantial energy differences between the contrast enhanced scans and the endogenous results.

Finally, although under-performing when compared to DMAS in terms of SMXR, the TGRCB algorithm achieves the best localization performance. Data-Independent beamformers rely on an assumed homogeneous channel model, while Data-Adaptive algorithms use collected signal data in order to overcome the inhomogeneous nature of the actual channel.

6. CONCLUSIONS

In this paper, four beamforming algorithms are evaluated on differential images obtained with the application of contrast agents in a heterogeneous imaging scenario. The contrast agents modify the dielectric properties of cancerous tissue within the breast, to increase the contrast between normal and cancerous tissues. Differential profiles represent the magnitude of energy-change from a scan with endogenous tumor properties and a scan with a contrast agent applied. Two contrast agents were investigated: microbubbles and SWCNT. In order to adequately examine the performance of each beamformer, 12 3D FDTD models were created, each with a malignant microlobular inclusion of different size. All beamforming algorithms were examined using two metrics: SMXR and D_{rel}.

For both contrast agents, all beamformers successfully located a scatterer embedded within a region of fibroglandular tissue when differential images were obtained. Significantly, tumors as small as 2 mm are readily identified within the differential images. The DMAS algorithm achieves the highest SMXR metric results. DMAS effectively exploits the contrast in the dielectric properties of an endogenous and contrast enhanced malignant scatterer, emphasising the difference in the resultant energy levels of each scan. The TGRCB algorithm achieves the highest D_{rel} metric results. Large perturbations in the assumed homogeneous channel affect the ability

of a Data-Independent beamformer to accurately locate the tumor. Data-Adaptive beamformers attempt to compensate for the actual, dielectrically diverse channel by using the received signal data to determine appropriate weights for filtering. Future work will involve using more effective antenna compensation techniques as well as investigating contrast-enhanced imaging in extremely dense heterogeneous breast models.

ACKNOWLEDGMENT

This work is sponsored by IRCSET and Hewlett Packard, under the Enterprise Partnership Scheme.

REFERENCES

1. AMC, "Cancer facts and figures 2009," Tech. Rep., American Cancer Society, 2009.
2. Nass, S. L., I. C. Henderson, and J. C. Lashof, *Mammography and Beyond: Developing Technologies for the Early Detection of Breast Cancer*, National Academy Press, 2001.
3. Huynh, P. H., A. M. Jarolimek, and S. Daye, "The false-negative mammogram," *RadioGraphics*, Vol. 18, 1137–1154, 1998.
4. Hagness, S. C., A. Taflove, and J. E. Bridges, "Two-dimensional fdtd analysis of a pulsed microwave confocal system for breast cancer detection: Fixed focus and antenna array sensors," *IEEE Transactions on Biomedical Engineering*, Vol. 45, 1470–1479, 1998.
5. Meaney, P. M., M. W. Fanning, D. Li, S. P. Poplack, and K. D. Paulsen, "A clinical prototype for active microwave imaging of the breast," *IEEE Transactions on Microwave Theory and Techniques*, Vol. 48, 1841–1853, 2000.
6. Lazebnik, M., L. McCartney, D. Popovic, C. B. Watkins, M. J. Lindstrom, J. Harter, S. Sewall, A. Magliocco, J. H. Booske, M. Okoniewski, and S. C. Hagness, "A large-scale study of the ultrawideband microwave dielectric properties of normal breast tissue obtained from reduction surgeries," *Physics in Medicine and Biology*, Vol. 52, 2637–2656, 2007.
7. O'Halloran, M., M. Glavin, and E. Jones, "Effects of fibroglandular tissue distribution on data-independent beamforming algorithms," *Progress In Electromagnetics Research*, Vol. 97, 141–158, 2009.
8. Byrne, D., M. O'Halloran, M. Glavin, and E. Jones, "Data independent radar beamforming algorithms for breast cancer

detection," *Progress In Electromagnetics Research*, Vol. 107, 331–348, 2010.

9. Mashal, A., B. Sitharaman, J. Booske, and S. Hagness, "Dielectric characterization of carbon nanotube contrast agents for microwave breast cancer detection," *IEEE Antennas and Propagation Society International Symposium, 2009. APSURSI'09*, 1–4, June 2009.
10. Fear, E. C., X. Li, S. C. Hagness, and M. A. Stuchly, "Confocal microwave imaging for breast cancer detection: Localization of tumors in three dimensions," *IEEE Transactions on Biomedical Engineering*, Vol. 47, 812–812, 2002.
11. Lim, H. B., N. T. T. Nhung, E.-P. Li, and N. D. Thang, "Confocal microwave imaging for breast cancer detection: Delay-multiply-and sum image reconstruction algorithm," *IEEE Transactions on Biomedical Engineering*, Vol. 55, No. 6, 1697–1704, June 2008.
12. Klemm, M., I. Craddock, J. Leendertz, A. Preece, and R.Benjamin, "Improved delay-and-sum beamforming algorithm for breast cancer detection," *International Journal of Antennas and Propogation*, Vol. 2008, 9, 2008.
13. Byrne, D., M. O'Halloran, E. Jones, and M. Glavin, "Transmitter-grouping robust capon beamforming for breast cancer detection," *Progress In Electromagnetic Research*, Vol. 108, 401–416, 2010.
14. Guo, B., Y. Wang, J. Li, P. Stoica, and R. Wu, "Microwave imaging via adaptive beamforming methods for breast cancer detection," *Journal of Electromagnetic Waves and Applications*, Vol. 20, No. 1, 53–63, 2006.
15. Xie, Y., B. Guo, L. Xu, J. Li, and P. Stoica, "Multi-static adaptive microwave imaging for early breast cancer detection," *IEEE Transactions on Biomedical Engineering*, Vol. 53, 1647–1657, 2006.
16. Maeda, H., "The enhanced permeability and retention (epr) effect in tumor vasculature: The key role of tumor-selective macromolecular drug targeting," *Advan. Enzyme Regul.*, Vol. 41, 189–207, 2001.
17. Mashal, A., J. H. Booske, and S. C. Hagness, "Toward contrast-enhanced microwave-induced thermoacoustic imaging of breast cancer: An experimental study of the effects of microbubbles on simple thermoacoustic targets," *Physics in Medicine and Biology*, Vol. 54, 641–650, 2008.
18. Sitharaman, B. and L. J. Wilson, "Gadofullerenes and gadonanotubes: A new paradigm for high-performance magnetic resonance imaging contrast agent probes," *Journal of Biomedical Nanotechnology*, Vol. 3, 342–352, December 2007.

19. Mashal, A., B. Sitharaman, X. Li, P. K. Avti, A. V. Sahakian, J. H. Booske, and S. C. Hagness, "Toward carbon-nanotube-based theranostic agents for microwave detection and treatment of breast cancer: Enhanced dielectric and heating response of tissue-mimicking materials," *IEEE Transactions on Biomedical Engineering*, Vol. 57, No. 8, 1831–1834, August 2010.
20. McDevitt, M. R., D. Chattopadhyay, B. J. Kappel, J. S. Jaggi, S. R. Schiffman, C. Antczak, J. T. Njardarson, R. Brentjens, and D. A. Scheinberg, "Tumor targeting with antibody-functionalized, radiolabeled carbon nanotubes," *J. Nucl. Med.*, Vol. 48, No. 7, 1180–1189, 2007.
21. Zastrow, E., S. K. Davis, M. Lazebnik, F. Kelcz, B. D. V. Veen, and S. Hagness, "Development of anatomically realistic numerical breast phantoms with accurate dielectric properties for modeling microwave interactions with the human breast," *IEEE Transactions on Biomedical Engineering*, Vol. 55, No. 12, 2792–2800, December 2008.
22. Muinonen, K., "Introducing the gaussian shape hypothesis for asteroids and comets," *Astronomy and Astrophysics*, Vol. 332, 1087–1098, 1998.
23. Conceicao, R. C., M. O'Halloran, M. Glavin, and E. Jones, "Support vector machines for the classification of early-stage breast cancer based on radar target signatures," *Progress In Electromagnetics Research B*, Vol. 23, 311–327, 2010.
24. Conceicao, R. C., M. O'Halloran, E. Jones, and M. Glavin, "Investigation of classifiers for early-stage breast cancer based on radar target signatures," *Progress In Electromagnetics Research*, Vol. 105, 295–311, 2010.
25. Okoniewski, M., M. Mrozowski, and M. A. Stuchly, "Simple treatment of multi-term dispersion in FDTD," *IEEE Microwave and Guided Wave Letters*, Vol. 7, 121–123, 1997.
26. Gabriel, C., S. Gabriel, and E. Corthout, "The dielectric properties of biological tissues: I. Literature survey," *Phys. Med. Biol.*, Vol. 41, No. 11, 2231–2249, Nov. 1996.
27. Shea, J. D., P. Kosmas, S. C. Hagness, and B. D. V. Veen, "Three dimensional microwave breast imaging: A bounded, multi frequency inverse scattering solution on a uniform voxel mesh," *Proceedings of the 2008 URSI General Assembly*, France, 2008.
28. Sacks, Z., D. Kingsland, R. Lee, and J. Lee, "A perfectly matched anisotropic absorber for use as an absorbing boundary condition," *IEEE Transactions on Antennas and Propagation*, Vol. 43, No. 12, 1460–1463, 1995.